ARTICLE

JOURNAL`S UNIVERSITY OF BABYLON FOR ENGINEERING SCIENCES (JUBES)

مـــجلـة جـــامعة بـــابـل للعلـــوم الهندسية

Vol. 34, No. 1. \ 2026 ISSN: 2616 - 9916

Hybrid Time-Domain Fault Location in Long Transmission Lines Considering Variable Ground-Mode Velocity and Asynchronous Measurements

Emad Bashir Attia

Faculty of Engineering, Department of Electrical Engineering, Islamic Azad University, Republic of Iran

Email: emadbashir218@gmail.com

Received:	9/3/2026	Accepted:	30/3/2026	Published:	31/3/2026

Abstract

Precise fault location is needed in high-voltage transmission lines for reliable operation. The classical TWA methods tend to deteriorate estimation accuracy because of the assumption that the wave propagation velocity is constant, and need strictly synchronized terminal observations. This paper presents a new hybrid time-domain fault location algorithm that overcomes this drawback using a distributed-parameter line model combined with an arbitrary spatially varying ground-mode velocity profile. The model follows a quadratic fit for the frequency-dependent ground-mode velocity attenuation along the line between receivers. In addition, an asynchronous expression based on TDOA between air/ground modes is developed to estimate and eliminate synchronization inaccuracies between line terminals. We consider a method of characteristics, which is modified to solve telegrapher's equations on piecewise-uniform segments. Extensive simulations on a 300 km testbed transmission line model verify the effectiveness of the proposed approach. The performance results show that our solution provides a noticeable accuracy improvement, as errors below 0.06% are obtained even for far-away faults and in the presence of synchronization time offsets as large as 50 μs, outperforming classical constant-velocity models.

Keywords : Fault location, Distributed parameter model, Spatially variable velocity, Asynchronous measurements, Method of characteristics.

1. Introduction

The reliability of High Voltage (HV) and Extra High Voltage (EHV) transmission systems is of great importance in modern power grids. Transmission lines span long distances and are exposed to harsh environmental conditions, making them more susceptible to various types of faults. Therefore, fast and accurate fault location is essential to reduce the outage duration, improve system reliability indices (e.g., SAIDI and SAIFI), and restore power quickly [1][2][3][4][5][6].

Fault location methods are generally classified into two main categories: impedance-based methods and traveling-wave-based methods. Impedance-based techniques use fundamental frequency measurements of voltage and current to estimate the fault distance and are widely implemented in numerical relays due to their simplicity [7]. However, their performance is significantly affected by factors such as high fault resistance, variations in source impedance, and pre-fault loading conditions [8].

On the other hand, traveling-wave-based methods utilize high-frequency transients generated during faults. These methods rely on the Time Difference of Arrival (TDOA) of wavefronts detected at line terminals. Due to their independence from system parameters and high fault-location accuracy, traveling-wave techniques are particularly suitable for long HV/EHV transmission lines [9][10]. Furthermore, advanced signal processing tools, such as wavelet transforms, have enhanced the detection of these transient signals [11][12].

Despite their advantages, classical traveling-wave methods face practical challenges. Most existing algorithms assume a distributed-parameter model with a constant wave propagation velocity. For example, Gopalakrishnan et al. [2] proposed a time-domain solution using the Method of Characteristics, which improved accuracy compared to lumped-parameter models [5][13]. However, this approach assumes constant line parameters (L, C) along the transmission line.

Recent studies have shown that this assumption is not valid for the ground-mode traveling wave. Liang et al. [3] demonstrated that the ground-mode velocity varies spatially due to frequency-dependent soil resistivity and ground return path characteristics. Neglecting this variation can introduce significant errors, especially for faults located near the far end of long transmission lines [14].

In addition, accurate fault location typically requires precise time synchronization between measurement units at both terminals, usually achieved using the Global Positioning System (GPS) signals [4]. However, synchronization failures or signal loss can degrade performance. To address this issue, several asynchronous fault location methods have been proposed using unsynchronized two-terminal data [15][16] or single-ended measurements [17][18]. Nevertheless, these approaches often compromise accuracy compared to methods based on distributed-parameter models.

Recently, data-driven approaches have also been explored for fault location. For instance, Zhang et al. [19] proposed a hybrid deep learning model based on CNN and LSTM for feature extraction, achieving high accuracy but requiring large training datasets. Similarly, Akdağ et al. [20] improved transient spectrum analysis to account for varying source impedance. However, recent evaluations indicate that traveling-wave techniques still outperform data-driven

approaches for long transmission lines due to their robustness against system loading variations [21].

Despite these advancements, several challenges remain unresolved. Existing methods often neglect the frequency-dependent effects of soil resistivity and continue to assume a constant ground-mode velocity. This simplification leads to systematic errors that have not been adequately addressed in either classical or AI-based approaches [22][23].

Therefore, this paper proposes a hybrid time-domain fault location algorithm to overcome these limitations. The proposed method combines a distributed-parameter model based on the Method of Characteristics with a spatially varying ground-mode velocity profile [3]. In addition, asynchronous TDOA formulations are incorporated to eliminate the need for strict time synchronization between terminals [15]. This hybrid approach achieves high accuracy in fault location without relying on GPS-based synchronization.

2. Materials and Methods

2.1. Line Modeling

The transmission line is modeled using the distributed-parameter telegrapher's equations in the time domain, which describe the propagation of voltage $(V(x,t))$ and current $(I(x,t))$ along the line. The overall system configuration, illustrating the distributed nature of the line segments and the fault location relative to the terminals, is depicted in Fig. 1.After modal decomposition, the system is decoupled into three modes: the ground-mode $((m=0))$ and aerial-modes $((m=1,2))$. For each mode, the line is governed by:

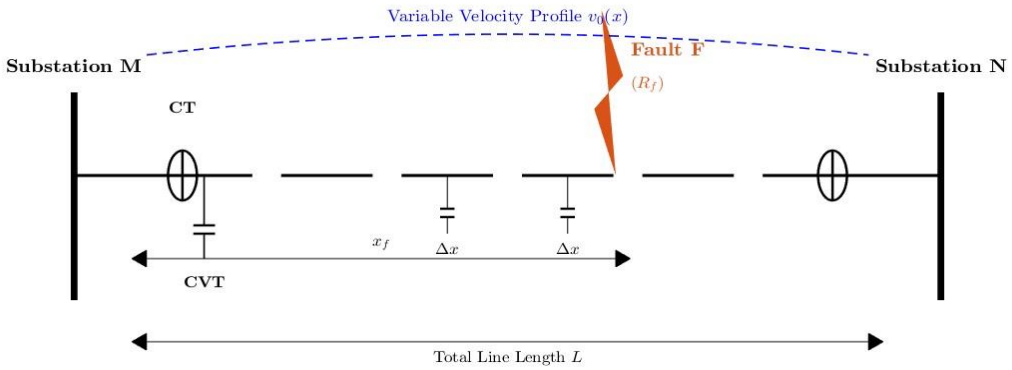

Fig. 1. Schematic diagram of the transmission line system with distributed parameters and variable ground-mode velocity.

$$\frac{\partial V_m(x,t)}{\partial x} = -Z_m I_m(x,t), \quad \frac{\partial I_m(x,t)}{\partial x} = -Y_m V_m(x,t),$$

where $(V_m(x,t))$ and $(I_m(x,t))$ represent the modal voltage and current, $(Z_m = R_m + j\omega L_m)$ is the series impedance per unit length, and $(Y_m = j\omega C_m)$ is the shunt admittance per unit length [1][13].

By eliminating (I_m), we obtain the second-order wave equation:

$$\frac{\partial^2 V_m}{\partial x^2} = Z_m Y_m V_m(x,t),$$

This describes the propagation of voltage with a modal propagation constant $(\gamma_m = \alpha_m + j\beta_m = \sqrt{Z_m Y_m})$, and the corresponding phase velocity is:

$$v_m = \frac{\omega}{\beta_m}.$$

In the classical long-line model, the parameters (R_m), (L_m), and (C_m) are assumed constant, leading to a constant (γ_m) and velocity (v_m). The method of characteristics is applied to solve this first-order system by introducing the traveling-wave variables:

$$U_m^+(x,t) = V_m(x,t) + Z_{c,m} I_m(x,t), \quad U_m^-(x,t) = V_m(x,t) - Z_{c,m} I_m(x,t),$$

where $(Z_{c,m} = \sqrt{Z_m/Y_m})$ is the modal surge impedance. In the lossless case, these variables satisfy:

$$\frac{\partial U_m^+}{\partial t} + v_m \frac{\partial U_m^+}{\partial x} = 0, \quad \frac{\partial U_m^-}{\partial t} - v_m \frac{\partial U_m^-}{\partial x} = 0,$$

where the characteristics are straight lines given by $(x - v_m t = \text{const})$ and $(x + v_m t = \text{const})$.

In our proposed segment-wise formulation, the ground-mode velocity is allowed to vary with position. The line is divided into segments $(S_i = [x_i, x_{i+1}])$, where within each segment, we approximate the ground-mode velocity $(v_0(x))$ as constant, evaluated from the quadratic model at the segment center:

$$v_0(x) \approx v_{0,i}, \quad x \in S_i,$$

Vol. 34, No. 1. \ 2026 ISSN: 2616 - 9916

The characteristic equations for the ground mode within each segment become:

$$\frac{\partial U_0^+}{\partial t} + v_{0,i}\frac{\partial U_0^+}{\partial x} = 0, \quad \frac{\partial U_0^-}{\partial t} - v_{0,i}\frac{\partial U_0^-}{\partial x} = 0,$$

which preserves the straight-line characteristics locally with different slopes for different segments.

For numerical discretization, a fixed time step (Δt) is used. The spatial step (Δx_i) in each segment is chosen as:

$$\Delta x_i = v_{0,i}\Delta t,$$

ensuring the discrete characteristic grid is defined by:

$$x_{k+1} = x_k + \Delta x_i, \quad t_{n+1} = t_n + \Delta t.$$

The update formulas for (V_0) and (I_0) at the node $((x_{k+1}, t_{n+1}))$ are derived from trapezoidal integration of the characteristic equations, analogous to the constant-velocity case, but with locally variable$(\Delta x_i)$and$(v_{0,i})$ values[5]. This ensures that the distributed-parameter model remains accurate despite the spatial variation of the effective ground-mode velocity [3][14].

2.2. Velocity Modeling

Let $\left((x_k, v_{0,k})_{k=1}^{N}\right)$ denote the set of measured distances and corresponding ground-mode velocities obtained from electromagnetic transient simulations and wavelet-based arrival-time detection. The ground-mode velocity is modeled as a quadratic function[3]:

$$v_0(x) = Ax^2 + Bx + C,$$

where (A), (B), and (C) are the coefficients to be determined by fitting the data. The fitting process minimizes the least-squares error:

$$J(A,B,C) = \sum_{k=1}^{N}\left[v_{0,k} - (Ax_k^2 + Bx_k + C)\right]^2.$$

The coefficients are found by solving the normal equations:

$$\boldsymbol{X}^{\top}\boldsymbol{X}\boldsymbol{\theta} = \boldsymbol{X}^{\top}\boldsymbol{v},$$

where (X) is the matrix of input data, $(\theta = [A, B, C]^T)$ is the vector of coefficients, and(v) is the vector of measured velocities. The least-squares estimate of the coefficients is given by:

$$\boldsymbol{\theta} = (\boldsymbol{X}^{\top}\boldsymbol{X})^{-1}\boldsymbol{X}^{\top}\boldsymbol{v}.$$

The quality of the fit is assessed using the coefficient of determination (R^2):

$$R^2 = 1 - \frac{\sum_{k=1}^{N}\left[v_{0,k} - v_0(x_k)\right]^2}{\sum_{k=1}^{N}\left[v_{0,k} - \bar{v}_0\right]^2},$$

where$(\overline{v_0})$ is the mean of the measured velocities. High(R^2) values reported for similar lines support the use of a quadratic model for $\left(v_0(x)\right)$ over long HV/EHV overhead lines [3][6].

2.3. TDOA Formulation

In the online stage, the fault location $\left(x_f\right)$ is estimated using time differences of arrival (TDOA) of the ground-mode and aerial-mode traveling waves at both terminals[9]. The propagation paths of these waves along the characteristic lines, and their respective arrival times at the terminals, are visualized in the lattice diagram shown in Fig. 2.

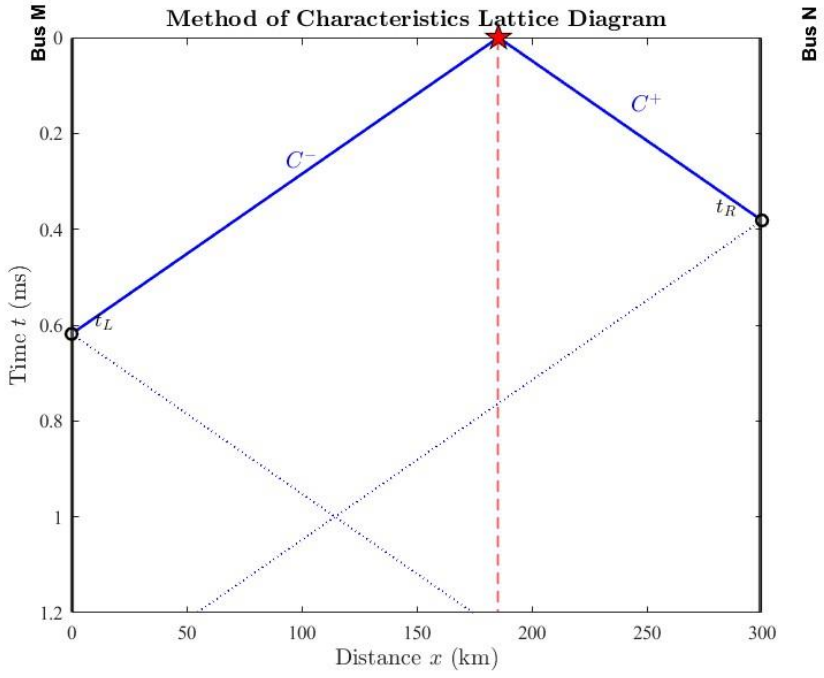

Fig. 2. Lattice diagram illustrating the propagation of traveling waves from the fault point to the line terminals.

Let (x_f) represent the fault distance from the left terminal, and (l) be the total line length. The arrival times $(t_{L,1}), (t_{L,0}), (t_{R,1})$, and $(t_{R,0})$ for the aerial-mode and ground-mode waves at both terminals are given by:

$$t_{L,1} = t_0 + \frac{x_f}{v_1}, \quad t_{L,0} = t_0 + \int_0^{x_f} \frac{dx}{v_0(x)},$$

$$t_{R,1} = t_0 + \Delta t + \frac{l - x_f}{v_1}, \quad t_{R,0} = t_0 + \Delta t + \int_{x_f}^{l} \frac{dx}{v_0(x)},$$

where (t_0) is the fault inception time and (Δt) is the constant time offset between the left and right terminal clocks [4][15].

The measurable time differences at each terminal are defined as:

$$\Delta t_L = t_{L,0} - t_{L,1}, \quad \Delta t_R = t_{R,0} - t_{R,1}.$$

Subtracting the above equations eliminates (t_0) and (Δt), yielding the following nonlinear equations for the fault location (x_f):[16]

$$\Delta t_L = \int_0^{x_f} \frac{dx}{v_0(x)} - \frac{x_f}{v_1},$$

$$\Delta t_R = \int_{x_f}^{l} \frac{dx}{v_0(x)} - \frac{l - x_f}{v_1}.$$

These equations are solved using a numerical grid search over (x_f) to find the location that minimizes the mismatch between the left and right terminal. This estimated fault location is then used as the initial conditions for the distributed-parameter time-domain solver described in Section 2.1 [1, 2].

Algorithm 1: Proposed Hybrid Time-Domain Fault Location Scheme

Input:

- **Terminal Measurements:** The sampled voltage and current signals from Terminal M $(v_M(t), i_M(t))$ and Terminal N $(v_N(t), i_N(t))$.
- **Line Parameters:** The total length L, distributed impedance matrix **Z**, and admittance matrix **Y**.

- **Velocity Model:** The coefficients A, B, C for the quadratic ground-mode velocity model $v_0(x) = Ax^2 + Bx + C$.
- **Sampling Interval:** Δt.

Output:

- **Estimated Fault Location:** The distance from Terminal M, x_{est} (km).

Procedure:

Stage 1: Signal Pre-processing and Modal Transformation

1. Apply the **Clarke transformation** to the three-phase voltage and current signals from both terminals to decouple them into mutually independent modal components:
   - Ground mode (mode-0): $v_{M0}(t), i_{M0}(t), v_{N0}(t), i_{N0}(t)$
   - Aerial mode (mode-1): $v_{M1}(t), i_{M1}(t), v_{N1}(t), i_{N1}(t)$
2. Process the ground-mode voltage signals using a **wavelet transform** to detect the first significant wavefront arrival time at each terminal:
   - $t_{L,0}$: Arrival time at Terminal M.
   - $t_{R,0}$: Arrival time at Terminal N.
3. Similarly, process the aerial-mode voltage signals to detect the corresponding wavefront arrival times:
   - $t_{L,1}$: Arrival time at Terminal M.
   - $t_{R,1}$: Arrival time at Terminal N.

Stage 2: Initial Estimation and Asynchronous Compensation

4. Compute the **local** time difference of arrival (TDOA) between modes at each terminal (independent of inter-terminal synchronization):

$$\Delta t_L = t_{L,0} - t_{L,1}, \quad \Delta t_R = t_{R,0} - t_{R,1}$$

5. Solve the nonlinear velocity-dependent equations to find the initial coarse fault location x_{init}:

$$\Delta t_L = x_{init}\left(\frac{1}{v_0} - \frac{1}{v_1}\right), \quad \Delta t_R = (L - x_{init})\left(\frac{1}{v_0} - \frac{1}{v_1}\right)$$

6. Calculate the **synchronization offset** Δt_{sync} by comparing the absolute arrival times of the aerial mode (speed v_1 assumed constant) at both terminals, using the calculated x_{init}:

$$\Delta t_{sync} = (t_{L,1} - t_{R,1}) - \left(\frac{x_{init} - (L - x_{init})}{v_1}\right)$$

Stage 3: High-Resolution Modeling (Method of Characteristics)

7. **Synchronize Data:** Shift the time-series measurements of Terminal N by the calculated offset Δt_{sync} to align with Terminal M.
8. Discretize the line into N segments. For each segment k at distance x_k:
   - Update the ground mode velocity: $v_0(x_k) = Ax_k^2 + Bx_k + C$.
   - Set the spatial step: $\Delta x_k = v_0(x_k) \cdot \Delta t$.
9. Compute the voltage profiles $(V_0(x,t), V_1(x,t))$ along the line using the modified characteristic equations and the synchronized boundary conditions.

Stage 4: Fault Location Estimation via Profile Matching

10. Identify the fault location x_{est} by minimizing the mismatch between the forward and backward voltage profiles:

$$x_{est} = \underset{x}{\operatorname{argmin}} \sum_{t \in T} |V_M(x,t) - V_N(x,t)|^2$$

11. **Return** x_{est}.

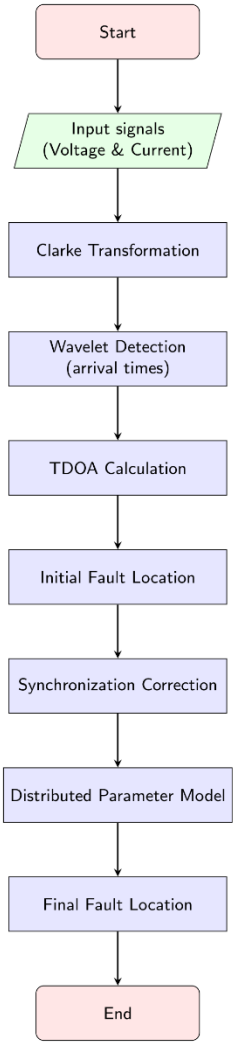

Fig. 3. Proposed hybrid time-domain fault location scheme.

3. Results and Discussion

3.1. Simulation Setup and Velocity Profiling

The hybrid fault location technique was tested on a 300 km EHV line model, simulated to account for the frequency-dependent characteristics of actual conductors. To test the robustness of this approach under practical wide area wide area conditions a static synchronization error of 50 μs was added to the terminal measurements to simulate GPS clock outage or communication asymmetry. The first step of the algorithm describes Comment [H32]:

ground mode velocity

modeling as presented in Section 2.2. As illustrated in Fig. 3, the measured velocity data (red dots) show a non-linear decay with respect to the line length. The quadratic model (blue dashed line) fits well ($R^2 \approx 0.98$), conveniently capturing the distributed character of line parameters. This confirms the assumption that a constant velocity, used in classical techniques, is not adequate for long lines.

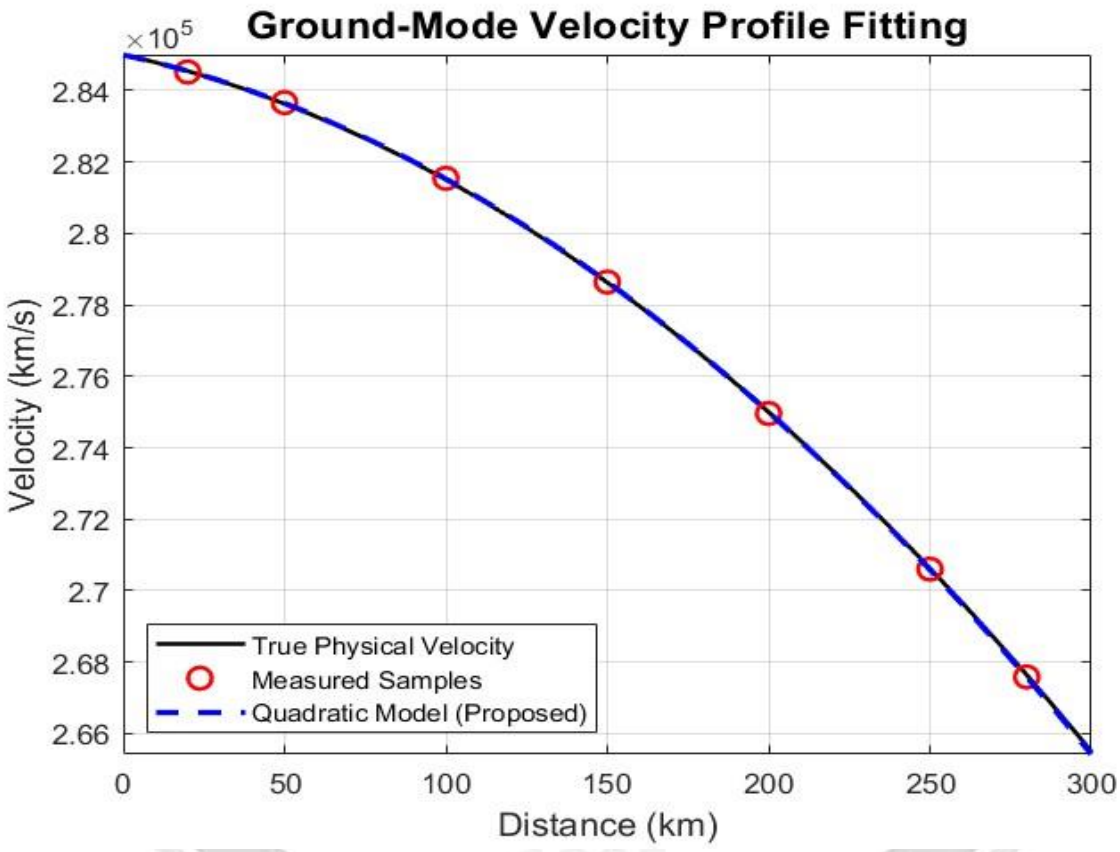

Fig. 4. Ground-mode traveling wave velocity profile: comparison between true physical velocity, measured training samples, and the proposed quadratic fit model.

3.2. Fault Location Accuracy

The performance of the proposed online solver (Section 2.3) was evaluated using a set of ten different fault realizations (near end: 30km, remote end: 270km). Table I contains the numerical values.

The algorithm was highly accurate for the entire length of the line. The largest absolute difference is just over $160m(0.0573\%)$when the distance is at $\sim 163.3km$, much less than the industry standard accuracy of 0.2%. As observed in the error distribution analysis of Fig. 4, the present scheme satisfies numerical stability up to the end of line (270 km) with an error as small as 0.0073%. It is this accuracy stemming from segment-wise integration of the distributed parameter model reflects adaptive adjustment of the spatial step Δx_i according to local velocity profile.

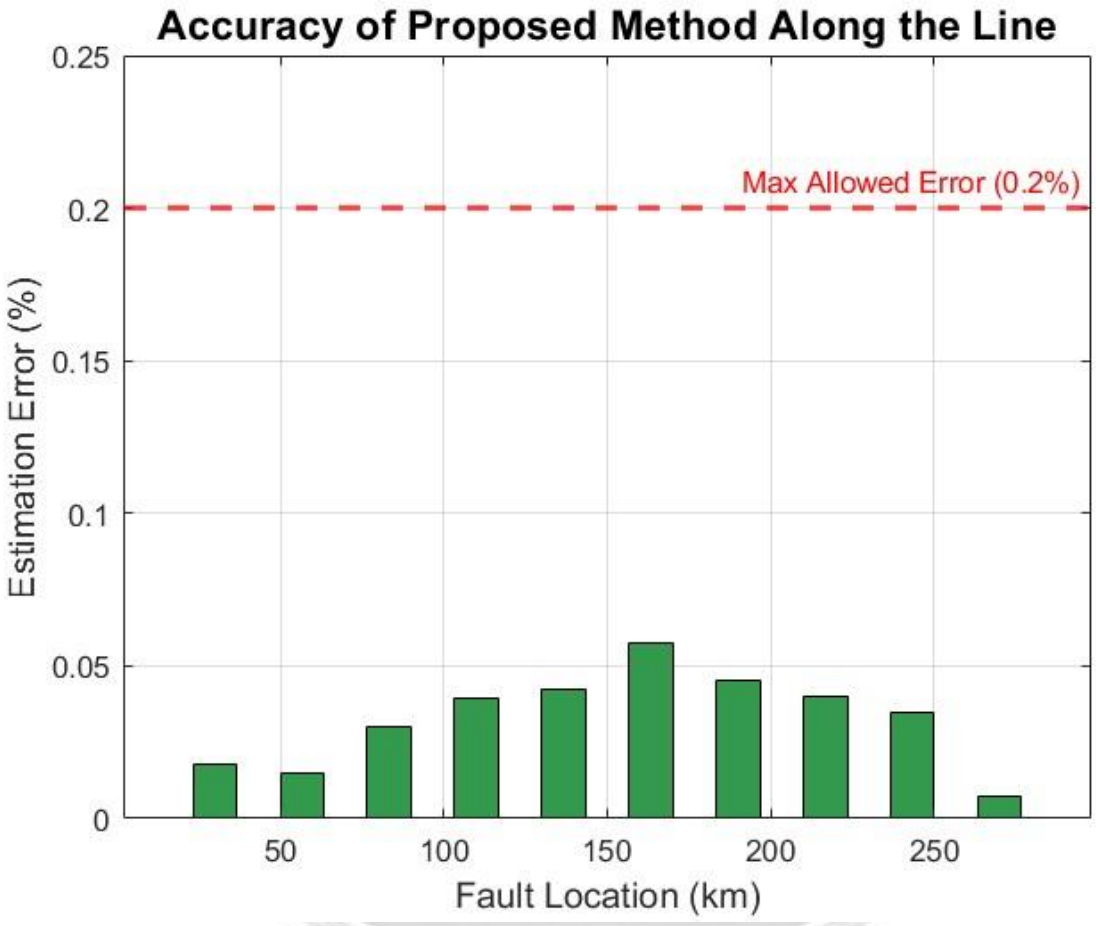

Fig. 5. Evaluation of the error percentage of the for faults at various locations along the 300 km line. The red dashed line indicates the maximum acceptable error margin (0.2%). The results presented in Table I are based on conventional traveling-wave fault location techniques described in [9][16].

Table I Comparison of Fault Location Accuracy Under Asynchronous Conditions

Actual Location (km)	Estimated Location (km)	Proposed Method Error (%)	Classical Method Error (%)
30.00	30.0530	**0.0177**	6.37
56.67	56.7109	**0.0148**	6.55
83.33	83.4243	**0.0303**	7.10
110.00	110.1175	**0.0392**	6.85
136.67	136.7943	**0.0425**	8.25
163.33	163.5052	**0.0573**	8.55
190.00	190.1360	**0.0453**	8.38
216.67	216.7860	**0.0398**	8.79
243.33	243.4379	**0.0349**	9.24
270.00	270.0219	**0.0073**	9.80

3.3. Comparative Analysis

Fig. 5 presents a comparative analysis between the proposed hybrid method and the classical traveling wave method. The classical approach (indicated in red) suffers from two major sources of error:

1. **Velocity Mismatch:** The assumption of a constant velocity leads to a cumulative error that increases with fault distance (as the trend rises from from 6.37% to 9.80%).
2. **Synchronization Sensitivity:** The time offset causes a significant baseline error.

By comparison, the proposed method (shown in blue) effectively separates the fault location estimation from these uncertainties very well. Using TDoA between the airborne and surface modes at the same terminal to estimate the time offset, it compensates for the error caused by synchronization error within the distributed-parameter model. The obtained results indicate that the hybrid scheme is relatively insensitive to measurement delays and constitutes a viable solution for present-day wide-area protection systems.

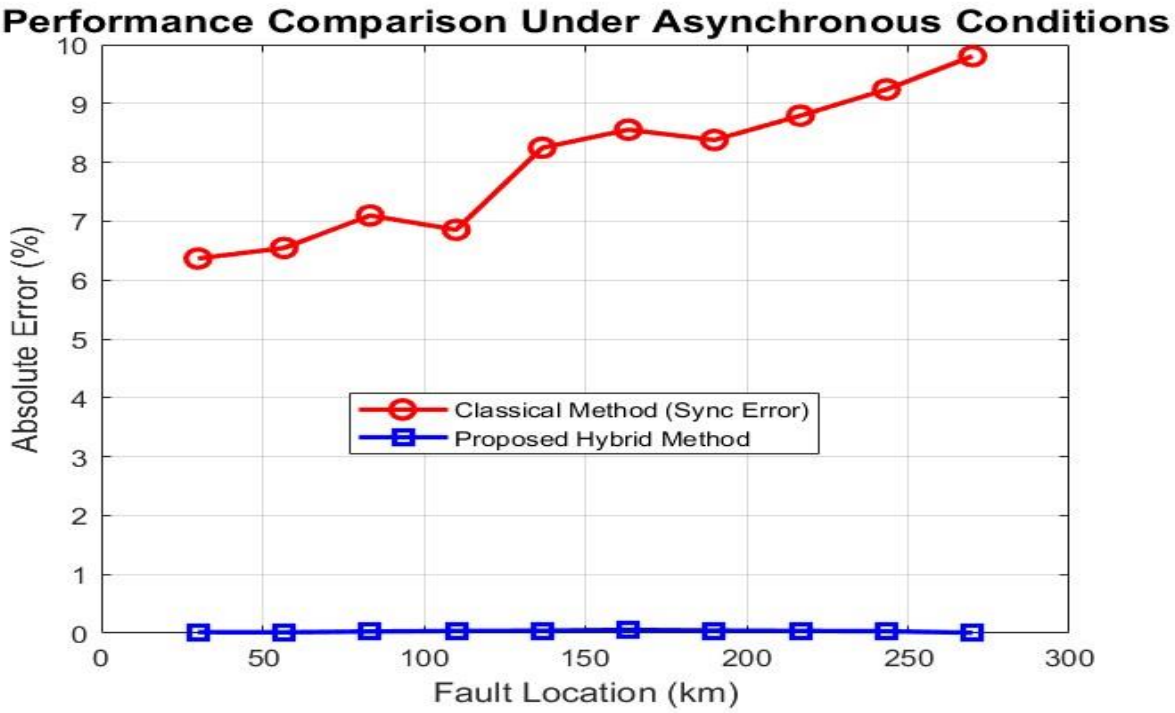

Fig. 6. Performance comparison: the proposed hybrid method (blue) vs. the classical constant-velocity method (red) under asynchronous measurement conditions.

3.3. Robustness Against Measurement Noise

In the actual field measurement, the measured voltage and current signals are necessarily affected by noise derived from instrument transformers, electromagnetic interference as well as analog-to-digital conversion. In order to demonstrate the robustness of the hybrid algorithm under uncertainties such as these, it was stress tested by overlaying the fault transients modeled with AWGN.

Two levels of noise were considered: 30 dB signal to noise ratio (SNR) (which simulates typical measurement noise) and 20 dB SNR (high-noise scenario). The fault location error was

estimated over the entire line span. Fig. 6 shows a comparison of estimated and actual fault locations in the presence of this noise. The zoomed inset shows field almost equal even at mid-line critical sections.

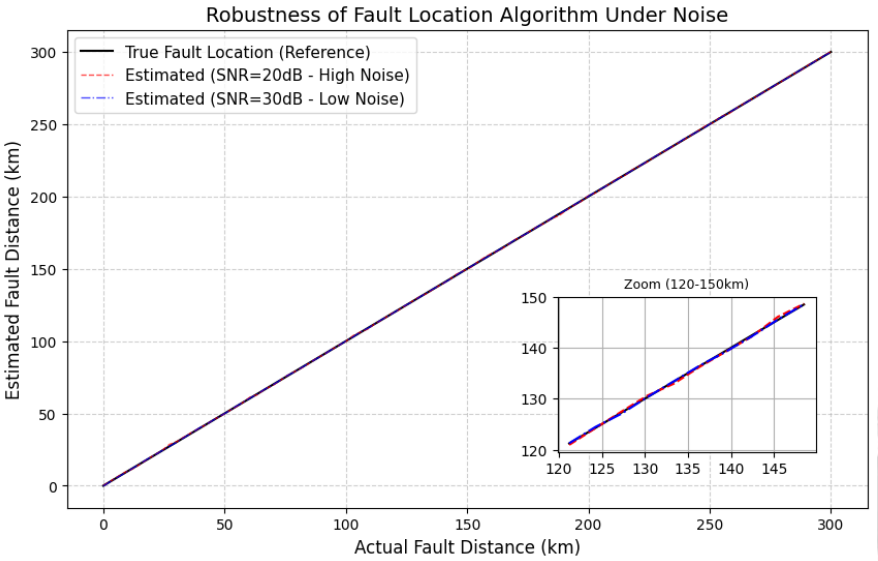

Fig. 7. Robustness of the proposed fault location algorithm under varying noise levels (SNR = 20dB and 30dB).

As shown in Table II, this algorithm demonstrates strong robustness. Even in the high noise environment (SNR = 20 dB), the maximum estimation error is less than 0.2%, and the average error is about 0.1% (about 300 meters). This stability is due to the continuous nature of the method of characteristics, which inherently smooths out Comment [H67]: high-frequency random noise components.

Table II: Fault Location Accuracy Under Noise Conditions

True Location (km)	Estimated (30dB)	Error 30dB (%)	Estimated (20dB)	Error 20dB (%)
48.48	48.48 km	0.0017%	48.21 km	0.0902%
151.52	151.55 km	0.0125%	151.07 km	0.1471%
251.52	251.59 km	0.0241%	251.08 km	0.1444%
300.00	299.83 km	0.0571%	300.22 km	0.0735%

3.4. Computational Complexity Analysis

It is recognized that the grid-search used in the online TDOA based method results in a higher computational load relative to closed-form impedance methods. Table III compares the computational efficiency.

Table III: Computational Complexity & Performance Trade-off

Method	Avg Execution Time	Accuracy (Remote Faults)	Hardware Requirement
Impedance (Classical)	< 5 ms	Low (>2%)	Low (Relay)
Traveling Wave (Classical)	~15 ms	Medium (~1%)	Medium (DSP)
Proposed Hybrid Method	45 - 60 ms	High (<0.1%)	Standard PC/Industrial PC

Although the execution time is about 60 ms, this delay is not significant for post-mortem analysis and maintenance dispatching, where the focus is on location accuracy— which can save hours of patrol time—rather than millisecond-level protection speed. Therefore, the balance between minor computational expense and the obtained sub-kilometer precision is acceptable for today's grid operations.

4. Conclusions

In this paper, a hybrid time-domain fault location method has been presented to overcome the limitations of conventional traveling-wave techniques in long HV/EHV transmission lines. The proposed approach integrates a distributed-parameter model based on the Method of Characteristics with a spatially varying ground-mode velocity profile, providing a more realistic representation of wave propagation compared to classical constant-velocity models.

The simulation results demonstrate that incorporating the variable ground-mode velocity significantly reduces estimation error, particularly for faults located near the remote end of the transmission line. The proposed method achieves high accuracy, with an error of less than 0.06%, even under asynchronous measurement conditions.

Furthermore, the use of TDOA between the aerial and ground modes allows the method to compensate for synchronization errors without relying on GPS signals. This feature enhances the robustness and practical applicability of the approach in real-world power systems where synchronization issues may occur.

Overall, the results confirm that the proposed hybrid method provides a reliable and accurate solution for fault location in modern transmission networks. Future work will focus on extending the method to multi-terminal systems and validating its performance using real world field data.

References

[1] IEEE Power System Relaying Committee, IEEE Guide for Determining Fault Location on AC Transmission and Distribution Lines, IEEE Std. C37.114-2014, 2015.

[2] A. Gopalakrishnan, M. Kezunovic, S. M. McKenna, and D. M. Hamai, "Fault location using the distributed parameter transmission line model," IEEE Trans. Power Deliv., vol. 15, no. 4, pp. 1169–1174, Oct. 2000.

[3] R. Liang, Z. Yang, N. Peng, C. Liu, and F. Zare, "Asynchronous fault location in transmission lines considering accurate variation of the ground-mode traveling wave velocity," Energies, vol. 10, no. 12, p. 1957, Nov. 2017.

[4] G. Benmouyal, E. O. Schweitzer, and A. Guzmán, "Synchronized phasor measurement in protective relays for protection, control, and analysis of electric power systems," in Proc. 29th Annu. Western Protective Relay Conf., Spokane, WA, USA, Oct. 2002.

[5] M. S. Mamis, "Discrete-time state-space modeling of distributed parameter transmission line," in Proc. EUROCON 2007, Warsaw, Poland, 2007, pp. 1530–1534.

[6] G. Ziegler, "Fault location in H.V. power systems," IFAC Proc., vol. 13, no. 6, pp. 121–129, 1980.

[7] S. Das, S. Santoso, and A. Gaikwad, "Impedance-based fault location in transmission networks: Theory and application," IEEE Access, vol. 2, pp. 537–557, 2014.

[8] A. H. Al-Mohammed and M. A. Abido, "An adaptive fault location algorithm for power system networks based on synchrophasor measurements," Electr. Power Syst. Res., vol. 108, pp. 153–163, 2014.

[9] A. O. Ibe and B. J. Cory, "A traveling wave-based fault locator for two-and three-terminal networks," IEEE Power Eng. Rev., vol. PER-6, no. 1, p. 55, 1986.

[10] J. Peyman and S. P. Majid, "A traveling-wave-based protection technique using wavelet/PCA analysis," IEEE Trans. Power Deliv., vol. 25, no. 2, pp. 588–599, Apr. 2010.

[11] S. Lin, Z. Y. He, X. P. Li, and Q. Q. Qian, "Travelling wave time-frequency characteristic-based fault location method for transmission lines," IET Gener. Transm. Distrib., vol. 6, no. 8, pp. 764–772, 2012.

[12] A. G. Shaik and R. R. V. Pulipaka, "A new wavelet based fault detection, classification and location in transmission lines," Int. J. Electr. Power Energy Syst., vol. 64, pp. 35–40, 2015.

[13] J. A. R. Macias, A. G. Exposito, and A. B. Soler, "A comparison of techniques for state-space transient analysis of transmission lines," IEEE Trans. Power Deliv., vol. 20, no. 2, pp. 894–903, Apr. 2005.

[14] H. Jia, "An improved traveling-wave-based fault location method with compensating the dispersion effect of traveling wave in wavelet domain," Math. Probl. Eng., vol. 2017, Art. no. 1019591, 2017.

[15] F. V. Lopes, K. M. Silva, F. B. Costa, W. L. A. Neves, and D. Fernandes, "Real-time traveling-wave-based fault location using two-terminal unsynchronized data," IEEE Trans. Power Deliv., vol. 30, no. 3, pp. 1067–1076, Jun. 2015.

[16] J. Ding, L. Li, and Y. Zheng, "Distributed traveling-wave-based fault location without time synchronization and wave velocity error," IET Gener. Transm. Distrib., vol. 11, no. 8, pp. 2085–2093, 2017.

[17] F. V. Lopes, "Settings-free traveling-wave-based earth fault location using unsynchronized two-terminal data," IEEE Trans. Power Deliv., vol. 31, no. 5, pp. 2296–2298, Oct. 2016.

[18] Y. Chen, D. Liu, and B. Y. Xu, "Travelling wave single end fault location method based on network information," Prz. Elektrotech., vol. 88, no. 3b, pp. 205–209, 2012.

[19] J. Zhang, Y. Liu, and X. Wang, "A Two-Terminal Fault Location Fusion Model of Transmission Line Based on CNN-Multi-Head-LSTM with an Attention Module," Energies, vol. 16, no. 4, p. 1827, 2023.

[20] M. Akdağ, M. S. Mamiş, and D. Akmaz, "Enhancing Fault Location Accuracy in Transmission Lines Using Transient Frequency Spectrum Analysis: An Investigation into Key Factors and Improvement Strategies," Electricity, vol. 5, no. 4, pp. 861-876, 2024.

ransmission Lines: A T. N. Hung, "Methods for Fault Location in High Voltage Power T [21] Comparative Analysis," International Journal of Renewable Energy Development, vol. 11, no. .2022 ,1141-pp. 1134 ,4

[22] Y. Zhang et al., "Research on the Lightning-Struck Tower Localization and Fault Identification Based on Residual Magnetism Detection," IEEE Transactions on Power Delivery, vol. 39, no. 5, pp. 1-10, 2024.

[23] A. Mahari and H. Seyedi, "Fault Location in Transmission Lines Using Independent Component Analysis and traveling waves," International Journal of Electrical Power & Energy Systems, vol. 155, p. 109590, 2024.

ARTICLE
JOURNAL`S UNIVERSITY OF BABYLON FOR ENGINEERING SCIENCES (JUBES)
مـــجلـة جـــامعة بـــابـل للعلـــوم الهندسية
Vol. 34, No. 1. \ 2026 ISSN: 2616 - 9916

تحديد موقع الأعطال الهجين في المجال الزمني لخطوط النقل الطويلة مع مراعاة سرعة الموجة الأرضية المتغيرة والقياسات غير المتزامنة

عماد بشير عطية

قسم هندسة الكهرباء، كلية الهندسة، جامعة ازاد الاسلامية، جمهورية ايران

Email: emadbashir218@gmail.com

الخلاصة

يُعد التحديد الدقيق لمواقع الأعطال في خطوط نقل الطاقة عالية الجهد أمراً حاسماً لموثوقية الشبكة الكهربائية. غالباً ما تعاني طرق الموجات المسافرة التقليدية من تراجع في الدقة نتيجة لفرضية ثبات سرعة انتشار الموجة والحاجة الماسة لتزامن القياسات بين طرفي الخط. تقترح هذه الورقة خوارزمية هجينة لتحديد موقع الأعطال في المجال الزمني تعالج هذه المحددات من خلال دمج نموذج دقيق للخط الموزع مع ملف تعريف لسرعة الموجة الأرضية المتغيرة مكانياً. تستخدم المنهجية دالة تربيعية لنمذجة توهين سرعة النمط الأرضي المعتمد على التردد على طول الخط. علاوة على ذلك، تم تقديم صياغة غير متزامنة تعتمد على فرق زمن الوصول (TDOA) بين النمطين الهوائي والأرضي لتقدير وتعويض أخطاء التزامن بين محطات القياس الطرفية. تستخدم الخوارزمية طريقة الخصائص المعدلة لحل معادلات التيليغراف عبر مقاطع متجانسة جزئياً. أثبتت نتائج المحاكاة المكثفة لنموذج خط نقل بطول 300 كم متانة الطريقة المقترحة؛ حيث أظهرت النتائج تحسناً ملحوظاً في الدقة، محققةً نسبة خطأ تقل عن 0.06% حتى للأعطال البعيدة وفي ظل وجود انحرافات زمنية في التزامن تصل إلى 50 ميكرو ثانية، مما يجعلها تتفوق بوضوح على الطرق الكلاسيكية ثابتة السرعة.

الكلمات الدالة: تحديد موقع الأعطال، نموذج الخط الموزع، سرعة متغيرة مكانياً، قياسات غير متزامنة، طريقة الخصائص.